Laminar Burning Velocity Measurements for an Outwardly Propagating Flame of Dimethyl Carbonate and Air Mixtures

Henriksen M.[1]*, Vaagsaether K.[1], Gaathaug A.V.[1], Lundberg J.[1], Forseth S.[2], Bjerketvedt D.[1]

[1] *University of South-eastern Norway, Faculty of Technology, Natural Sciences and Maritime Sciences, Porsgrunn, Telemark, Norway*

[2] *Norwegian Defence Research Establishment (FFI), Oslo, Norway*

**Corresponding author's email: mathias.henriksen@usn.no*

ABSTRACT

The electrolyte is one of the main components in a Li-Ion cell/battery. It consists of one or a mixture of organic carbonates (e.g., dimethyl carbonate) together with a Li-ion salt. The heat of combustion of the organic carbonates can contribute between 65-70% of the total energy content in a 18650 Li-ion cell. If a cell is heated, either by an external source or due to short-circuit, it may cause the battery to vent and, under certain conditions, experience thermal runaway. The laminar burning velocity is an essential parameter for flame propagation. It is also an essential input parameter for several computational fluid dynamic (CFD) codes. No experimental studies on laminar burning velocities are currently published for Li-ion electrolytes such as dimethyl carbonate (DMC). In this study, the Markstein length, the laminar flame speed and burning velocity for DMC and propane are determined for an outwardly propagating spherical flame (OPF). The flame was analyzed in a 20-liter explosion sphere with initial conditions at 100 kPa absolute and 300 K. The results from the experiments fit well with previously published results for propane and are slightly lower than theoretical calculation for DMC. Propane has higher laminar burning velocity compared to DMC, which corresponds well with the higher rate of explosion pressure rise for propane. DMC has a higher maximum explosion pressure compared to propane.

KEYWORDS: Laminar burning velocity, dimethyl carbonate, Li-ion battery electrolyte, gas explosion.

NOMENCLATURE

A	area (m^2)
K_G	deflagration index (bar m^3/s)
L	Markstein length (mm)
p	pressure (kPa, MPa)
r	radius (m, mm)
R^2	coefficient of determination
S	flame speed (m/s)
T	temperature (K)
t	time (ms)

Greek

ρ	density (kg/m^3)
κ	Stretch rate (1/s)
σ	density ratio
ϕ	Fuel- air equivalence ratio (-)

Subscripts

b	relative to burnt gas
ex	maximum explosion pressure for particular experiment
f	flame
u	relative to unburnt gas

Superscripts

0	laminar

Proceedings of the Ninth International Seminar on Fire and Explosion Hazards (ISFEH9), pp. 161-172
Edited by Snegirev A., Liu N.A., Tamanini F., Bradley D., Molkov V., and Chaumeix N.
Published by St. Petersburg Polytechnic University Press
ISBN: 978-5-7422-6496-5 DOI: 10.18720/spbpu/2/k19-29

INTRODUCTION

Li-ion batteries are popular when it comes to electrochemical energy storage due to its high energy density and specific energy compared to other rechargeable batteries [1]. In the last two decades, there have been several reports of fire and explosion related incidents caused by Li-ion battery failure [2]. Most of the flammable material comes from the electrolyte which is one of the main components in a Li-Ion cell/battery. It consists of one or a mixture of organic carbonates (e.g., Dimethyl carbonate) together with a Li-ion salt. According to an estimate from Mikolajczak, et al. [3], the heat of combustion of the organic carbonates contributes between 65-70% of the total energy content in a 18650 Li-ion cell, depending on the state of charge (SOC). In contrast, the electrical energy for the same cell is only 8-13% of the total energy depending on SOC.

From a safety point of view, this chemical/combustible energy is a potential hazard, especially for large battery systems found in electric vehicles, ships and power storage for smart grids. Overcharge, heat exposure, overdischarge, external and internal short-circuit are potential causes for batteries to become unstable and release a combustible gas mixture. The combustible gas mixture can be the solvent from the electrolyte and a mixture of hydrocarbons gases [1-9]. Fig. 1 shows two still images of an inhomogeneous propagating flame, from the released gas/mist vented from an externally heated 18650 Li-ion cell.

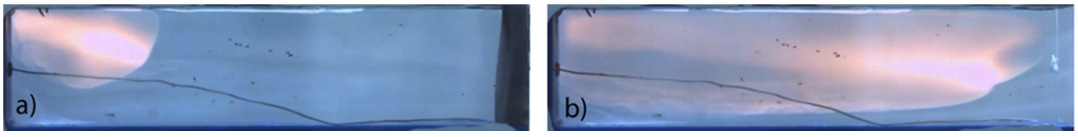

Fig. 1. Two still images of an inhomogeneous flame propagating inside a 0.45x0.10x0.10 explosion channel. A 18650 Li-ion cell was externally heated until the combustible gas/mist vented. a) Short after the ignition. b) Image when the flame has reached the end of the channel

Laminar burning velocity is an essential parameter for flame propagation. A flame will usually start slow and laminar with velocities in order of 0.5 m/s. As the flame propagates, it may become turbulent due to concentration differences, obstacles, self-generated turbulence and more [10]. For hydrocarbons, the higher laminar burning velocity usually corresponds to a more reactive mixture with a higher rate of explosion pressure rise. The laminar burning velocity is also an essential input parameter for several computational fluid dynamics (CFD) codes (e.g., Gülder formulation, [11]). No experimental studies on laminar burning velocities are currently published for Li-ion electrolytes such as dimethyl carbonate (DMC).

Laminar flame speed, burning velocity and Markstein lengths for DMC and propane for an outwardly propagating flame (OPF) are determined in a standard 20-liter explosion sphere. The experiments are performed in a typical manner as described in other studies [12-18]. Results from the propane experiments are compared with previously published studies and for DMC with a theoretical calculation. Initial conditions for all experiments were 100 kPa absolute and 300 K.

MATERIALS AND METHOD

Experimental setup and procedure

Figure 2 shows a schematic of the experimental setup. The vessel is a standard 20-liter explosion sphere. A heating jacket controls the internal temperature, and there is a heating plate in the bottom for liquid evaporation (not shown in schematics). Two Kistler 601CAA pressure transducers measured the explosion pressure at 125 kHz. A Keller PAA-33X pressure transducer recorded the pressure during the filling process to get the partial pressures for each component. Separate injection

ports/inlets for all materials were used to reduce uncertainties in the fuel-air concentration. The ignition system consists of an ignition coil with a primary inductance of 8.0±15% mH. Two metal wires with a diameter 1 mm, with a variable gap between them of 0.5 and 2.0 mm, is connected to the ignition coil. By charging the ignition coil with 12 volts, a spark with approximate 100 mJ and 30 000 V was generated. A focused shadowgraphy technique [19] was used to enhance the visibility of the propagating flame and was recorded with a Photron SA-Z high-speed camera operating at 20 000 frames per second (fps). An image processing tool generated in Matlab was used to analysis the shadowgraph images. The DMC had a purity above 99% and propane a purity above 99.95%.

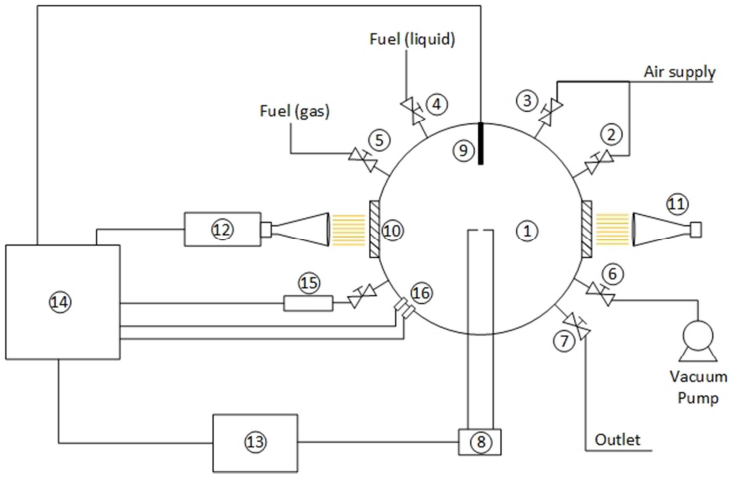

Fig. 2. Schematic of experimental setup. 1 explosion chamber, 2 oxidizer inlet, 3 flush inlet, 4 fuel (liquid) injection port, 5 fuel (gas) inlet, 6 vacuum port, 7 gas outlet, 8 ignition system, 9 thermocouple, 10 glass windows (100 mm), 11 LED light source, 12 high speed camera, 13 control/trigger unit, 14 data acquisition system, 15, ambient pressure sensor, 16 dual explosion pressure sensors

The explosion sphere was purged with compressed and oil-free air for a minimum of five minutes before each experiment. The explosion sphere was evacuated to an absolute pressure of 5 kPa (±0.2 kPa) after purging. Fuel was filled to the desired partial pressure, and then the sphere was filled with air to 100 kPa (±0.5 kPa). Air and fuel were actively mixed for five minutes to ensure a homogenous mixture. After mixing, the temperature was recorded. The temperature difference between experiments was within ±3.0 K. The ignition was delayed an additional three minutes after mixing to ensure that the mixture was quiescent. After ignition, the explosion pressure and high-speed recording were stored for further analysis.

For experiments that included liquid injections, the heating plate was set 10 K above the internal temperature of the explosion sphere to increase evaporation rate. There is a dip tube from the injection port down to a heating plate to ensure that the liquid enters on the heating plate. To reduce the risk of condensation and liquid residue, the maximum partial pressure of DMC was 8.2 kPa (DMC vapor pressure @ 300 K). After one to two minutes of constant pressure and no visible liquid residue in the vessel, the procedure continued as described above.

Outwardly propagating spherical flame method

In this study, the outwardly propagating spherical flame method was used to determine the flame speed (S_b). In each shadowgraph image, the flame radius is measured and considered stationary. The calculated rate of increase in flame radius (dr/dt) is identified as the flame speed. Figure 3 shows an illustration of flame propagation and Eq. (1) shows how the flame speed was calculated by Eq. (1),

$$S_b = \frac{dr}{dt} \tag{1}$$

where S_b is flame speed (m/s), *dr/dt* is rate of change in flame radius (m/s).

The flame radius was found by using the intensity gradients in a shadowgraph image. These gradients distinguish the outer perimeters of the flame from the burnt and unburnt gas in the image. The gradient closest to the burnt phase was chosen as the perimeter for the flame. The perimeter of the flame was then fitted to a circle using least square minimization [20] to obtain the overall/average radius. All radii are then post-filtered with a Savitzky-Golay smoothing algorithm [21] to reduce noise from the image processing. Since the flame front is spherical/curved, it does not conform to the planar laminar flame speed (S_b^0). The stretch rate needs to be evaluated in order to determine the unstretched/planar laminar flame speed. Stretch rate is defined by Eq. (2) [22].

$$\kappa = \frac{1}{A}\frac{dA}{dt} = \frac{2}{r}\frac{dr}{dt} \tag{2}$$

where κ is the stretch rate (1/s), A is a flame area (m^2), *dA/dt* is the rate of change in flame area (m^2/s), r is flame radius (m), *dr/dt* is the rate of change in flame area (m/s)

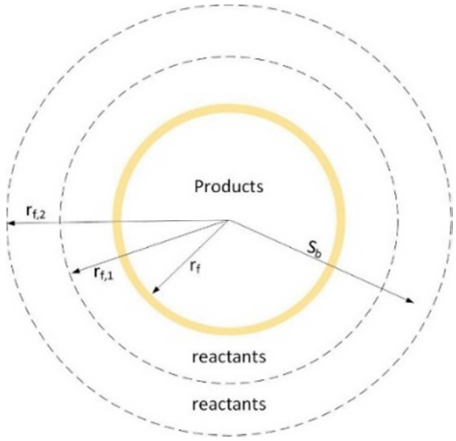

Fig. 3. Illustration of an outwardly propagating spherical flame.

In this study, the linear stretch model was used to determine the laminar flame speed (S_b^0) and the Markstein length (L_b). The linear expression is shown in Eq. (3).

$$S_b = S_b^0 + L_b\kappa \tag{3}$$

where, S_b is the flame speed with respect to the burnt mixture (m/s), S_b^0 is the laminar flame speed with respect to the burnt mixture (m/s), L_b is the Markstein length with respect to the burnt mixture, κ is the stretch rate (1/s)

From continuity and assuming quasi-steady flame, the laminar burning velocity (S_u^0) can be expressed by Eq. (4) [23].

$$S_u^0 = S_b^0 \cdot \frac{\rho_b}{\rho_u} = S_b^0\sigma \tag{4}$$

where, S_u^0, laminar burning velocity with respect to unburnt state (m/s), S_b^0, laminar flame speed with

respect to burnt state (m/s), ρ_b, density of equilibrium burnt state (kg/m^3), ρ_u, density of unburnt state (kg/m^3), σ, is the density ratio (-).

The chemical kinetics, thermodynamics, and transport process simulation tool Cantera (version 2.3.0) [24] was used to theoretically calculate laminar burning velocities and equilibrium states for constant pressure combustion. To calculate the laminar burning velocity the FreeFlame model was used with the same initial conditions as in the experiments. The FreeFlame model is a One-dimensional freely propagating planar flame with adiabatic conditions. The reaction mechanism for DMC was taken from Glaude et al. [25], and the Gri3.0 reaction mechanism for propane was from Smith et al. [26]. For density ration (σ) the constant pressure equilibrium solver was used. The established reaction mechanism for the different fuels provided the equilibrium constants and reaction sets for the calculation.

RESULTS AND DISCUSSION

Instabilities may influence the propagation of the flame and the flame speed due to thermal diffusion, hydrodynamic instabilities and buoyancy [13]. To reduce instabilities caused by thermal diffusion, and buoyancy effects, only concentrations closer to $\phi = 1.0$ was chosen. For some of the rich mixtures, small flame front instabilities can be seen in Fig. 4 and Fig. 5. These instabilities may cause small errors in the calculated laminar burning velocities. Regarding buoyancy effects, Ronney et al. reported that for laminar burning velocity above 0.15 m/s, the buoyancy would not affect the flame shape and not cause any significant errors in the radius measurements [27]. Discrepancies due to buoyancy are therefore considered to negligible.

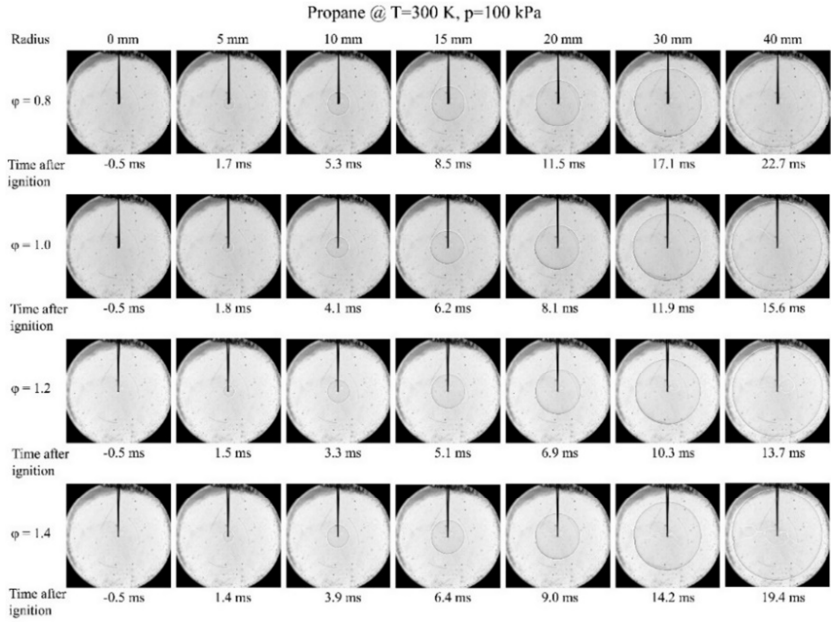

Fig. 4. Shadowgraph images of propane experiments. Flame propagation with radii from 0, 5, 10, 15, 20, 30 and 40 mm with corresponding time after ignition in milliseconds. Initial condition for experiments at 300 K and 100 kPa absolute

A change in pressure can cause hydrodynamic instabilities. There was no change in pressure in the time frame the flame speed was determined. Instabilities caused by a change in pressure was therefore not considered. Hydrodynamic instabilities can also be created during ignition.

Instabilities caused during ignition will often propagate along with the flame development [28] and be visible in the high-speed recording. Some experiments were rejected due to large instabilities from the ignition, which caused the flame to propagate none spherical. By varying the spark gap between 0.5 and 2.0 mm for different concentrations the ignition induced instabilities was reduced. By studying Fig. 4 and Fig. 5, the flame surface for most of the experiment is a smooth surface with relatively few instabilities.

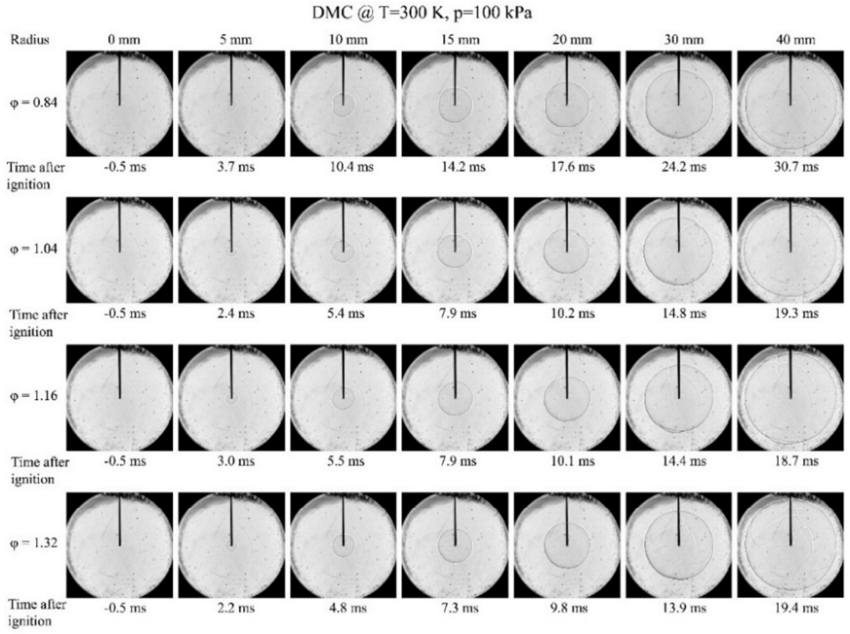

Fig. 5. Shadowgraph images of dimethyl carbonate (DMC) experiments. Flame propagation with radii from 0, 5, 10, 15, 20, 30 and 40 mm with corresponding time after ignition in milliseconds. Initial condition for experiments at 300 K and 100 kPa absolute.

Figure 6 shows the filtered flame radii and the calculated flame velocities as a function of time and radii for propane (left) and DMC (right). Figure a) and b) shows the filtered flame radii as a function of time. For experiments with ϕ above 1.0, the radius increases almost linearly with time. The radii were plotted with and without the filter applied to exclude over processing the data, but gave no significant difference in radii. Filtering was still applied to reduce fluctuations in the calculation of the flame speed. Liu et al. [18] reported similar linear trends for the propagation of the flame radius for propane with ϕ between 1.0 and 1.5.

The flame speed as a function of time is plotted in Fig. 6 c) and d) and as a function of flame radii in e) and d) for propane (left) and DMC (right). Due to small fluctuations between neighboring radii the change in the local speed can be substantial and therefore smoothed with a filter. The fluctuation between neighboring radii is caused by the pixel to meter resolution related to flame propagation. If the flame propagation is slow, the flame may be registered as almost stationary for two frames, before moving. Filtering this uneven propagation was chosen instead of curve fitting the data to a polynomial.

The flame has a higher acceleration between 5 and 10 mm than for the rest of the propagation. It is not clear what is causing this change, but Kelley et al. [28] reported similar results when studying critical radius for flame propagation. They reported that the flame accelerated until it reached expected flame speed and then propagate as expected. The acceleration occurred from the point of ignition to a flame radius of 10 mm, which is equal to what is observed in this study. Due to this

significant change in flame speed, the data below 10 mm was not used in the evaluation of the unstretched flame speed.

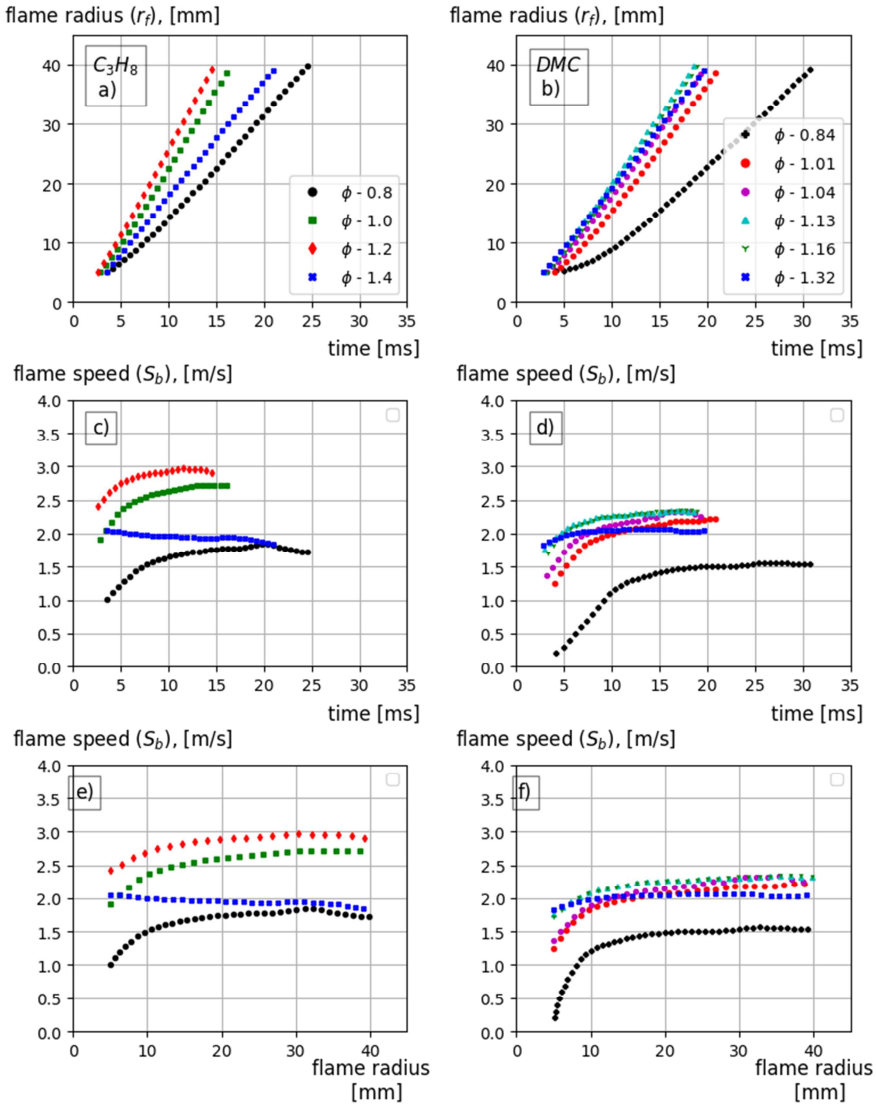

Fig. 6. Recorded data from shadowgraphy images and post-processing of images. a) and b) filtered radius as a function of time for propane and dimethyl carbonate respectively. c) and d), Calculated flame speed as a function of time for propane and dimethyl carbonate respectively. e) and f) Calculated flame speed as a function of filtered flame radius for propane and dimethyl carbonate respectively. Initial condition for all experiments was 300 K and 100 kPa absolute. The number of data point is reduced by a factor of 12 in the plots.

For propane and DMC there is a small and almost linear change in flame speed from 10 mm to 30 mm. Similar results have been reported for propane in previous studies [15, 18]. When the flame radius exceeds 30 mm, the flame speed changes for some of the concentrations. For propane, a small deceleration occurs for all expect $\phi = 0.99$. The flame speed for DMC does not have the same type of deceleration as propane. It is uncertain what the causes this change in flame speed. No pressure change was recorded as mention, so the pressure was not considered to be the cause. The

image processing could have issues at a radius exceeding 30 mm, due to the thresholding criteria. Further investigation of the data is needed to determine the cause. Radii above 30 mm were still used in the evaluation of laminar flame speed to have an equal length range for all experiments.

Figure 7 shows the flame speed as a function of the stretch rate for propane (left) and DMC (right). The data were fitted with a linear least square method to get the laminar flame speed and the Markstein length (L_b). There is some variation in how well the plotted data corresponded with the linear stretch model as shown in Fig. 7. The lowest coefficient of determination (R^2) for propane was 0.82 for ϕ=1.4 with an average value of 0.91. For DMC the lowest R^2 was 0.64 for ϕ = 1.32 with an average value of 0.92. The raw data points in Fig. 7 and Fig. 6 is reduced by a factor of 12 to avoid the points appearing as a complete line. All the raw data points are used in the least square minimization. For each experiment, the total number of data points fitted varied between 250 and 500 dependent on flame speed. By removing data with a radius above 30 mm would decrease the R^2, but not give any significant change in laminar flame speed and Markstein length.

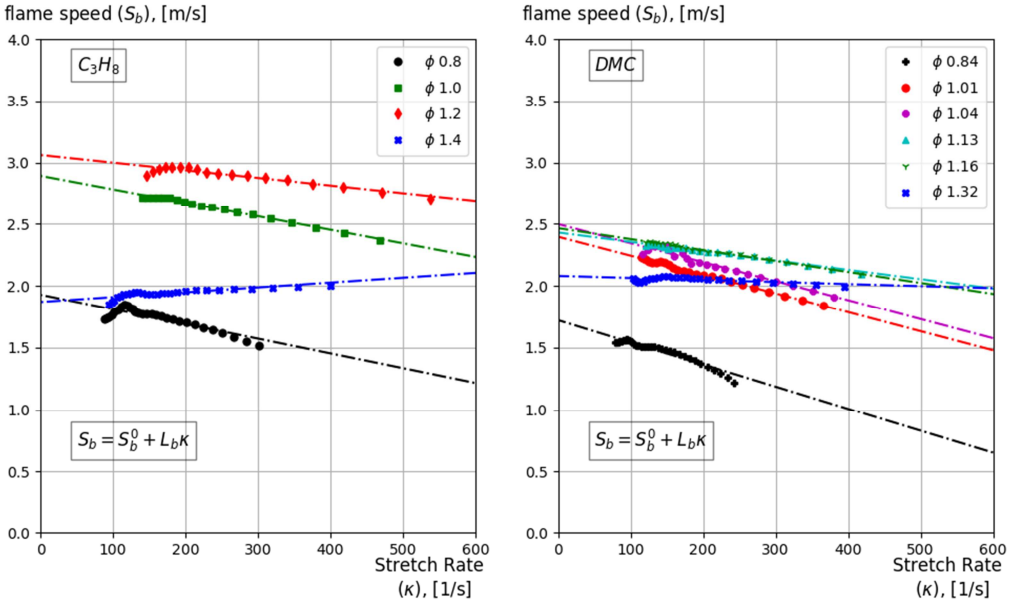

Fig. 7. Flame speed as a function of the stretch rate with the Linear stretch model as dashed lines for propane and dimethyl carbonate. Initial conditions for all experiments was 300 K and 100 kPa absolute. The number of data point is reduced by a factor of 12 in the plots.

Table 1 and Table 2 summarizes the results. Propane has the highest laminar burning velocity and flame speed at ϕ = 1.20. For DMC the highest laminar burning velocity and flame speed were found at ϕ = 1.04. For DMC the values are close to equal for $1.0 \leq \phi \leq 1.2$. For both fuels, the highest burning velocities are located near stoichiometric concentrations, with the highest values slightly on the rich side, which is expected. Figure 8 shows the propane results compared with previously published studies [14-18, 29] and the DMC results compared to the reaction mechanism from Glaude et al. [25]. The propane results compared very well with previously published results, which indicates that the experimental setup and method gives reasonable results. There is a discrepancy between the theoretical calculations and the experimental results for DMC. It is uncertain what is causing this discrepancy. According to Chen et al. [30], radiative heat loss can contribute to the discrepancy between simulations and experiments. Similar deviations were found in a recent study [31] where explosion characteristic (explosion pressure and rate of explosion pressure rise) was

measured. In this study, the explosion pressures for electrolytes were compared with theoretical calculation.

Table 1. Laminar flame speed, Markstein Length, and laminar burning velocity for propane at 300 K and 100 kPa absolute

Fuel-Air equivalence ratio	Laminar flame speed (S_b^0) [m/s]	Markstein length (L_b) [mm]	Laminar burning velocity (S_u^0) [m/s]
0.82	1.93	-1,19	0.27
0.99	2.89	-1.10	0.37
1.20	3.06	-0.62	0.39
1.43	1.87	0.39	0.25

Table 2. Laminar flame speed, Markstein Length, and laminar burning velocity for dimethyl carbonate (DMC) at 300 K and 100 kPa absolute

Fuel-Air equivalence ratio	Laminar flame speed (S_b^0) [m/s]	Markstein length (L_b) [mm]	Laminar burning velocity (S_u^0) [m/s]
0.84	1.72	-1.78	0.23
1.01	2.40	-1.53	0.29
1.04	2.50	-1.54	0.30
1.13	2.31	-0.76	0.29
1.16	2.47	-0.89	0.30
1.33	2.08	-0.17	0.25

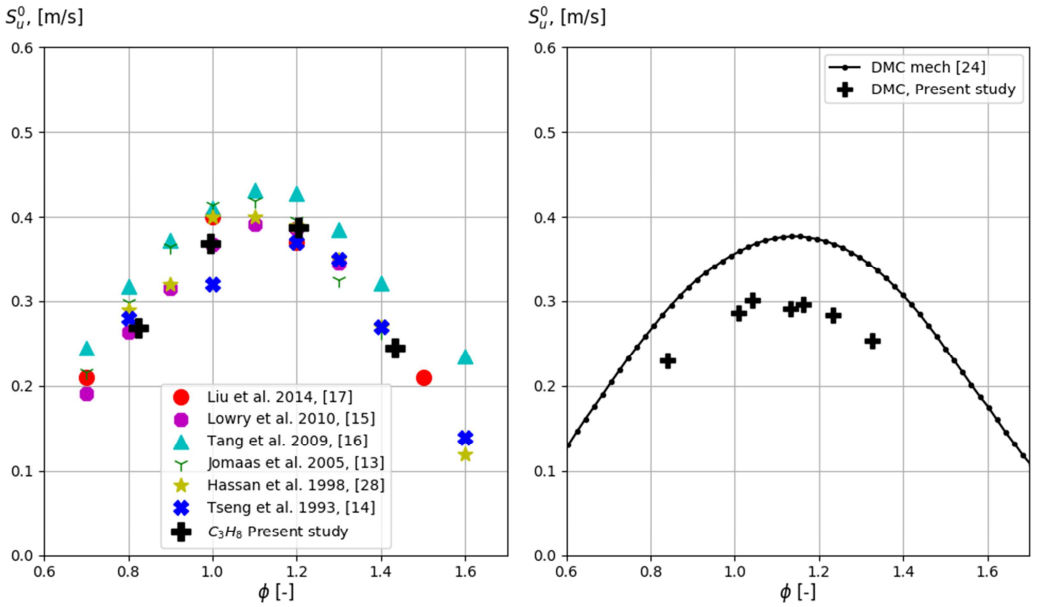

Fig. 8. A comparison of laminar burning velocity. Left) Propane laminar burning velocities compared to previously published results. Right) Dimethyl carbonate compared to reaction mechanism. Initial conditions for all experiments are 300 K and 100 kPa absolute.

Figure 9 shows a comparison of explosion pressure (left) and rate of explosion pressure rise (right) for propane and DMC. DMC has the highest explosion pressure of 938 kPa compared to propane. Propane had the highest rate of explosion pressure rise of 42.98 MPa/s of the two substances. The higher rate of explosion pressures for propane corresponds well with the burning velocity results. A recent study gave similar trends for propane and DMC with initial conditions at 373 K and 100 kPa [31]. For propane, there is more data point included in Fig. 9 than in Fig. 8. Figure 9 includes rejected experiments for laminar burning velocity due to a relatively high none spherical flame propagation.

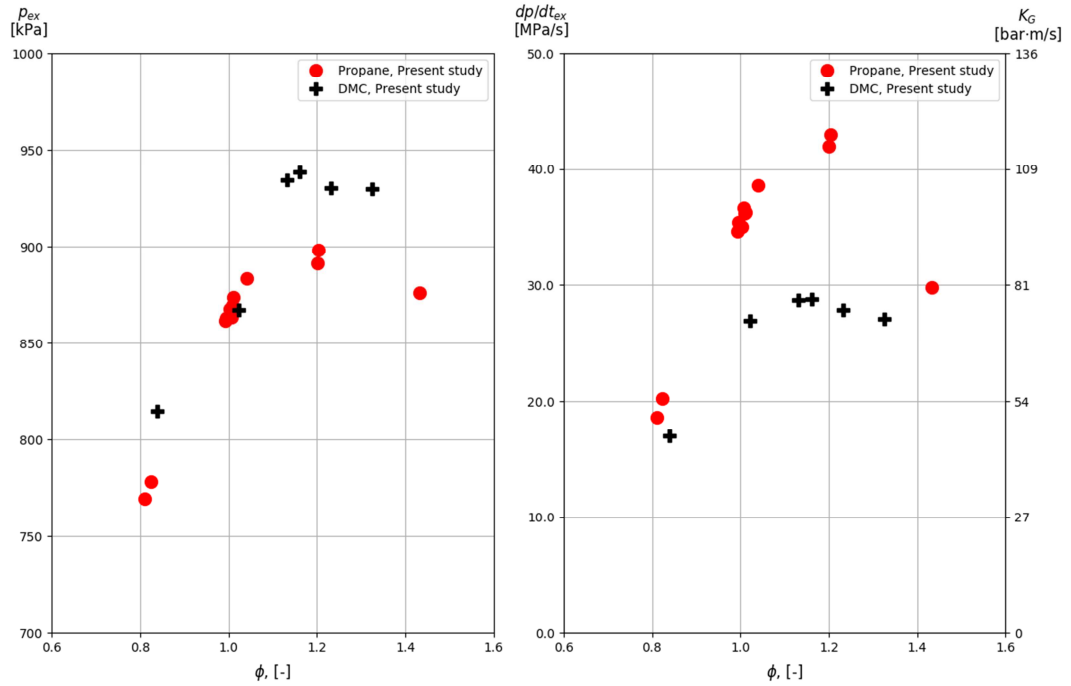

Fig. 9. A comparison of explosion characteristics for propane and dimethyl carbonate. Left) Comparison of explosion pressure. Right) Comparison of rate of explosion pressure rise. Initial conditions for all experiments is 300 K and 100 kPa absolute.

CONCLUSION

A 20-liter explosion sphere was used to determine the laminar flame speed, Markstein length and laminar burning velocity for propane and dimethyl carbonate at different concentrations, with the initial condition at 300 K and 100 kPa absolute. The procedure and experimental setup gave results consistent with previously published results and is considered a suitable method for determining laminar burning velocities.

An adiabatic and chemical equilibrium calculation performed using Cantera gave higher laminar burning velocities compared to experiments for DMC. This disagreement may be due to the radiative heat losses in the explosion sphere compared to the adiabatic conditions for the theoretical calculation. The maximum laminar burning velocity of 0.30 was found for fuel-air equivalence ratio of 1.04 for DMC.

DMC had the highest maximum explosion pressure of 938 kPa and propane largest rate of explosion pressure rise of 42.98 MPa/s. The maximum rate of explosion pressure rise for propane compared to DMC is consistent with propane higher burning velocities.

REFERENCES

[1] S. Abada, G. Marlair, A. Lecocq, M. Petit, V. Sauvant-Moynot, F. Huet, Safety focused modeling of lithium-ion batteries: A review, J. Power Sources. 306 (2016) 178–192.

[2] D. Lisbona, T. Snee, A review of hazards associated with primary lithium and lithium-ion batteries, Proc. Saf. Env. Protect. 89 (2011) 434–442.

[3] C. Mikolajczak, M. Kahn, K. White, R.T. Long, Lithium-Ion Batteries Hazard and Use Assessment, Springer US, Boston, MA, 2011.

[4] S.J. Harris, A. Timmons, W.J. Pitz, A combustion chemistry analysis of carbonate solvents used in Li-ion batteries, J. Power Sources. 193 (2009) 855–858.

[5] C.C. Crafts, D.H. Doughty, J. McBreen, E.P. Roth, Advanced technology development program for lithium-ion batteries : thermal abuse performance of 18650 Li-ion cells., 2004.

[6] B. Lei, W. Zhao, C. Ziebert, N. Uhlmann, M. Rohde, H. Seifert, Experimental Analysis of Thermal Runaway in 18650 Cylindrical Li-Ion Cells Using an Accelerating Rate Calorimeter, Batteries 3(2) (2017) 14.

[7] P. Ribière, S. Grugeon, M. Morcrette, S. Boyanov, S. Laruelle, G. Marlair, Investigation on the fire-induced hazards of Li-ion battery cells by fire calorimetry, Energy Environ. Sci. 5 (2012) 5271–5280.

[8] J. Johnsplass, M. Henriksen, K. Vaagsaether, J. Lundberg, D. Bjerketvedt, Simulation of burning velocities in gases vented from thermal run-a-way lithium ion batteries, in: Proceedings of the 58th SIMS, 2017, pp. 157–161.

[9] Q. Wang, P. Ping, X. Zhao, G. Chu, J. Sun, C. Chen, Thermal runaway caused fire and explosion of lithium ion battery, J. Power Sources. 208 (2012) 210–224.

[10] D. Bjerketvedt, J.R. Bakke, K. Van Wingerden, Gas explosion handbook, J. Hazard. Mater. 52 (1997) 1–150.

[11] O. Gülder, Correlations of Laminar Combustion Data for Alternative S.I. Engine Fuels, SAE Technical Paper (1984) 841000.

[12] A.A. Konnov, A. Mohammad, V.R. Kishore, N.I. Kim, C. Prathap, S. Kumar, A comprehensive review of measurements and data analysis of laminar burning velocities for various fuel+air mixtures, Progr. Energy Combust. Sci. 68 (2018) 197–267.

[13] F.N. Egolfopoulos, N. Hansen, Y. Ju, K. Kohse-Höinghaus, C.K. Law, F. Qi, Advances and challenges in laminar flame experiments and implications for combustion chemistry, Progr. Energy Combust. Sci. 43 (2014) 36–67.

[14] G. Jomaas, X.L. Zheng, D.L. Zhu, C.K. Law, Experimental determination of counterflow ignition temperatures and laminar flame speeds of C2–C3 hydrocarbons at atmospheric and elevated pressures, Proc. Combust. Inst. 30 (2005) 193–200.

[15] L.-K. Tseng, M.A. Ismail, G.M. Faeth, Laminar burning velocities and Markstein numbers of hydrocarbonair flames, Combust. Flame 95 (1993) 410–426.

[16] W. Lowry, J. de Vries, M. Krejci, E. Petersen, Z. Serinyel, W. Metcalfe, H. Curran, G. Bourque, Laminar Flame Speed Measurements and Modeling of Pure Alkanes and Alkane Blends at Elevated Pressures, J. Eng. Gas Turbines Power 133(9), 091501.

[17] C. Tang, J. Zheng, Z. Huang, J. Wang, Study on nitrogen diluted propane–air premixed flames at elevated pressures and temperatures, Energy Convers. Manage. 51 (2010) 288–295.

[18] Q. Liu, Y. Zhang, F. Niu, L. Li, Study on the flame propagation and gas explosion in propane/air mixtures, Fuel 140 (2015) 677–684.

[19] G.S. Settles, Schlieren and shadowgraph techniques: visualizing phenomena in transparent media, Springer, 2001.

[20] V. Pratt, Direct least-squares fitting of algebraic surfaces, ACM SIGGRAPH Computer Graphics, 21 (1987) 145–152.

[21] A. Savitzky, M.J.E. Golay, Smoothing and Differentiation of Data by Simplified Least Squares Procedures, Anal. Chem. 36 (1964) 1627–1639.

[22] F.A. Williams, Combustion Theory., Chapman and Hall/CRC, Boulder, 2018. http://public.eblib.com/choice/publicfullrecord.aspx?p=5320077 (accessed September 7, 2018).

[23] C.K. Law, Combustion Physics, Cambridge University Press, Cambridge ; New York, 2006.

[24] D.G. Goodwin, H.K. Moffat, R.L. Speth, Cantera: An Object-Oriented Software Toolkit For Chemical Kinetics, Thermodynamics, And Transport Processes. Version 2.3.0, (2017). doi:10.5281/zenodo.170284.

[25] P.A. Glaude, W.J. Pitz, M.J. Thomson, Chemical kinetic modeling of dimethyl carbonate in an opposed-flow diffusion flame, Proc. Combust. Inst. 30 (2005) 1111–1118.

[26] G.P. Smith, D.M. Golden, M. Frenklach, N.W. Moriarty, B. Eiteneer, M. Goldenberg, C.T. Bowman, R.K. Hanson, S. Song, W.C.G. Jr, V.V. Lissianski, Z. Qin, GRI-MECH 3.0, (n.d.). http://www.me.berkeley.edu/gri_mech/ (accessed March 18, 2018).

[27] P.D. Ronney, H.Y. Wachman, Effect of gravity on laminar premixed gas combustion I: Flammability limits and burning velocities, Combust. Flame 62 (1985) 107–119.

[28] A.P. Kelley, G. Jomaas, C.K. Law, Critical radius for sustained propagation of spark-ignited spherical flames, Combust. Flame 156 (2009) 1006–1013.

[29] M.I. Hassan, K.T. Aung, O.C. Kwon, G.M. Faeth, Properties of Laminar Premixed Hydrocarbon/Air Flames at Various Pressures, J. Propul. Power. 14 (1998) 479–488.

[30] Z. Chen, On the accuracy of laminar flame speeds measured from outwardly propagating spherical flames: Methane/air at normal temperature and pressure, Combust. Flame 162 (2015) 2442–2453.

[31] M. Henriksen, K. Vaagsaether, J. Lundberg, S. Forseth, Explosion characteristics for Li-ion Battery electrolytes at elevated temperatures, Under Review in J. Hazard. Mater., 2018.